Sensors & Actuators: A. Physical 337 (2022) 113443

Contents lists available at ScienceDirect

Sensors and Actuators: A. Physical

journal homepage: www.journals.elsevier.com/sensors-and-actuators-a-physical

Temperature-dependent photonic properties of porous-shaped metal-organic frameworks on porous silicon substrates

Shadi Ghafari, Nima Naderi *, Mohamad Javad Eshraghi, Mahmood Kazemzad

Materials and Energy Research Center, Karaj, Iran

ARTICLE INFO

Keywords:
Temperature-dependent photosensitivity
Photodetectors
Zeolitic imidazolate frameworks
Porous silicon
Solvothermal deposition
Metal-organic frameworks

ABSTRACT

A novel technique is introduced in this research to increase the surface roughness of metal-organic frameworks (MOF) to enhance the light absorption effect. To this end, porous silicon (PS) was selected as a template and zeolitic imidazolate frameworks (ZIF), a subset of MOFs, were deposited on the porous skeleton using the solvothermal method. It was found that the synthesized ZIF layers followed the physical pattern of porous silicon and developed a porous-shaped MOF thin film. The X-ray diffraction analysis proved the formation of polycrystalline ZIF-67 structures on the PS substrate with a dominant crystal orientation of (011). The SEM results showed the homogeneous formation of ZIF-67 on the top of the PS walls. The porous substrate provided sufficient nuclei for facilitating the formation of a compact and continuous ZIF top layer. Moreover, the morphology and crystalline properties of the PS substrate remained intact after the deposition of ZIF structures. The porous-shaped ZIF-67/PS sample exhibited an intense and sharp photoluminescence peak, reflecting its capability to capture the incident photon and generate electron-hole pairs. Thus, it can be regarded as a suitable candidate for light detection applications. The optoelectrical properties of the synthesized samples were further explored by the metallization of the ZIF/PS structures to fabricate metal–semiconductor–metal photodetectors whose current–voltage curves were measured upon exposure to different wavelengths. The photocurrent was found to be temperature-dependent with outstanding photosensitivity to ultraviolet radiation at lower temperatures. Therefore, porous-shaped ZIF-67 nanostructures on PS substrates can be a promising candidate for ultra-fast and highly sensitive UV detectors at low temperatures.

1. Introduction

Photodetectors are one of the most important components of optical integrated circuits to convert the optical signal into an electrical one. Numerous reports can be found on the fabrication and characterization of conventional photodetectors based on group III–V mineral semiconductors and silicon [1]. In the past few decades, organic semiconductors have received much attention for the fabrication of optical devices [2].

The optical devices based on inorganic semiconductors exhibit faster detection compared to those developed based on organic semiconductors. However, the fabrication of organic-based devices is less expensive. Therefore, a combination of two types of semiconductors can provide the advantage of both categories. For instance; the devices based on the combination of organic and inorganic semiconductors may offer faster detection at lower fabrication costs [3].

Metal-organic frameworks (MOFs), also known as coordination polymers, are a group of crystalline materials. The MOFs can be regarded as one, two, or three-dimensional lattice networks composed of metal ions linked by organic ligands [4]. The MOFs have exhibited interesting features such as extremely high surface area and tunable cavity size [5]. Moreover, they play decisive roles in different fields including gas storage and separation [6], luminescence materials [7], catalytic [8], magnetic [9], and drug delivery [10]. Regarding their multifunctional luminescence properties, these organic-inorganic hybrid materials can provide a versatile platform for luminescence generation. In MOFs, the metal–ligand charge transfer can add extra dimension to the photoluminescence functionality [11]; providing MOFs with the ability to generate various luminescence modes [12].

As a subset of MOFs, zeolitic imidazolate frameworks (ZIF) are composed of four quadratic intermediate metals such as zinc, cobalt, copper, and nickel connected to organic imidazolate binders within a quadrilateral arrangement. Compared to other types of MOFs, ZIF structures possess better thermal and chemical stability. The poor

* Corresponding author.
E-mail address: n.naderi@merc.ac.ir (N. Naderi).

https://doi.org/10.1016/j.sna.2022.113443
Received 22 November 2021; Received in revised form 16 January 2022; Accepted 7 February 2022
Available online 10 February 2022

electrical conductivity and low mechanical stability of pristine ZIFs have, however, limited their application in electronic industries. These drawbacks could be overcome by depositing ZIFs on a substrate. The combination of highly porous and adaptable structures due to the excellent compatibility of ZIFs with other nanoparticles can also promote several unique properties. Therefore, the deposition of ZIFs on different substrates can result in various optical and mechanical advantages [13].

One of the most feasible ways for deposition of ZIF thin films on a substrate is the solvothermal method which involves crystallization of dissolved species at high vapor pressures. In this technique, several reaction parameters (such as temperature, time, pH, and solvent type) can significantly influence the quality of the final product [14]. In this method, the reaction solution is a compound mixture of primary materials. The growth process occurs at the substrate surface and sometimes within the solution. This growth technique leads to the formation of polycrystalline films in which the crystals are attached to the surface of the substrate.

Porous silicon (PS) has drawn a huge deal of interest as a promising electronic substrate since the discovery of its dominant electrical and optical properties. The compatibility of porous silicon with silicon-based electronic technologies has promoted the development of different devices based on the PS [15]. The morphological and structural properties of PS nanostructures, as well as their optical and electrical performance, have been the subject of numerous studies [16]. Porous silicon has elevated internal surface area (~ 200–500 m^2 cm^{-3}); thus showing enhanced potential for increased adsorptive effects [17] which can be used in optical devices. The roughness of porous silicon can promote the adsorption of molecules and makes it a good substrate for the coating of optical materials [18].

In the current report, the porous structure of PS is chosen as a substrate to facilitate the formation of ZIF structures using the solvothermal method. Moreover, the obtained samples provide higher stability, larger surface-to-volume ratios, and improved optical properties. Therefore, the optimized ZIF thin films on PS substrates can be used in highly sensitive photodetectors.

2. Experiment

The PS structures were prepared using photoelectrochemical etching of n-type Si (100) with an electrical resistivity of 0.4 Ω cm. Before etching, silicon substrates were cleaned chemically by RCA cleaning technique. The resistivity of Si substrates showed a reduction to 36 mΩ cm after performing the RCA process. Gold thin film (~ 150-nm thick) was then sputter-coated on the back of the Si wafers and heated at 200 °C for 20 min under Ar flow to facilitate etching by reducing the resistivity to ~ 2 mΩ cm. The photoelectrochemical anodization was carried out for an etching time of 15 min under a 100 W tungsten lamp and at a current density of 30 mA cm^{-2}. The composition of chemical solution used here was hydrofluoric acid (HF; 38–40% w/w) and ethanol (C_2H_5OH; 96% w/w) in a volume ratio of 1:2. The etching process was facilitated by adding Genapol-PF-10 as a surfactant at the concentration of 0.3%(v/v).

Subsequently, ZIF-67 layers were synthesized on the porous skeleton of the optimized PS samples using the solvothermal technique. In a typical procedure, 291 mg cobalt (II) nitrate was dissolved in 16 mg of 2-methylimidazole which was separately dissolved in 5 mL of methanol. After complete dissolution of both compounds, PS substrates were placed in the solution containing the reagents, and the reactor was placed in an oven at 55 °C for 18 h. In order to study the impact of porous substrate, the same method was followed to synthesze ZIF-67 on as-cleaned monocrystalline Si substrate. Here, time of deposition was varied and the weight of samples was measured before and after deposition for obtaining the same amount of ZIF on the both substrates. A possible mechanism during the synthesis reaction of ZIF-67 structures involves the replacement of Co^{+2} metal ion sources. Here, the reaction

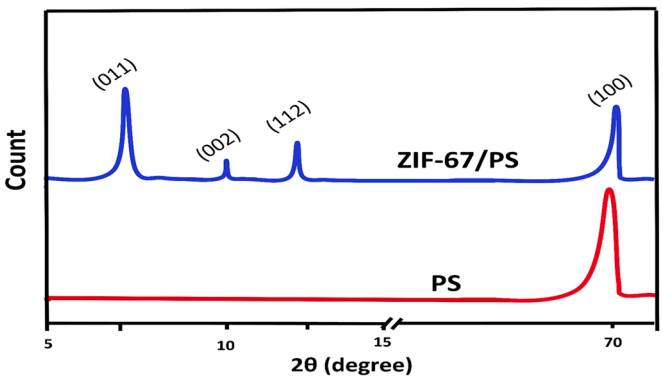

Fig. 1. XRD patterns of the bare PS and ZIF-67/PS nanostructures.

took place in contact with ligand molecules of 2-methyl imidazole in the solution at 60 °C.

Next, Au was sputtered to fabricate metal-semiconductor-metal (MSM) devices with two Schottky back-to-back contacts on ZIF layers. The distance between the two electrodes was minimized by applying a paired finger pattern (width: 50 μm, length: 2.8 mm, and separation distance:120 μm) using a metal mask. The exposed area of the fabricated devices was 0.1 cm^2. The optoelectronic properties of fabricated ZIF-67/PS-based photodetectors were measured using current-voltage characteristics upon exposure to different wavelengths and the darkness. The measurements indicated the temperature dependence of photocurrent. To study the effect of working temperature on the optoelectrical characteristics of the fabricated photodetectors, a thermoelectric cooling element (TEC1-12704) was applied at a voltage of 5 V and a current of 3.2 A to achieve the temperature difference of 50 °C. The devices showed better efficiency and higher sensitivity to the incident light at low temperatures.

The morphology of the substrates was also recorded using field emission scanning electron microscopy (FESEM, MIRA3TESCAN-XMU) at 30 kV. The structural characteristics were extracted using X-ray diffractometer (XRD, Phillips APD 3520) with Cu K-alpha radiation (40 keV, 30 mA). The PL analysis were performed using a spectrophotometer equipped with a laser diode source (300 nm, 20 mW) for excitation. The optoelectrical properties of the devices including their current-time (I–t) and current-voltage (I–V) curves were recorded using a source-measure equipment (Keithley 2400, USA) under different ambient temperatures.

3. Results and discussion

The structural properties of porous silicon substrate after and before deposition of ZIF-67 are illustrated in Fig. 1. The peak at $2\theta = 69.5°$ appeared in both samples can be assigned to the PS substrate with a crystal orientation of (100) according to the ICDD powder diffraction file with reference card no. 01-077-2109. Therefore, the crystalline structure of the PS substrate remained unchanged after the deposition of MOF. The working temperature of the solvothermal process was not elevated too much to destroy the crystal structure of Si walls in the PS samples. However, a slight decrease can be observed in the intensity of the PS peak due to the coverage of PS structures by ZIF thin films. The full width at half maximum (FWHM) of PS peak is 0.157° and 0.150° for PS and ZIF/PS samples, respectively. Therefore, the crystallite size of PS was almost preserved after the synthesis of ZIF structures. Three peaks appeared at $2\theta = 7.5°$, 10°, and 12.5° in the XRD pattern of ZIF/PS samples which can be related to ZIF-67 with different orientations of (011), (002) and (122), respectively [19]. The mentioned peaks indicated the formation of pristine ZIF structures on the top of the PS skeleton. The dominant peak at $2\theta = 7.5°$ suggests the (011) plane as the favorable orientation of ZIF formation for the growth of ZIF structures

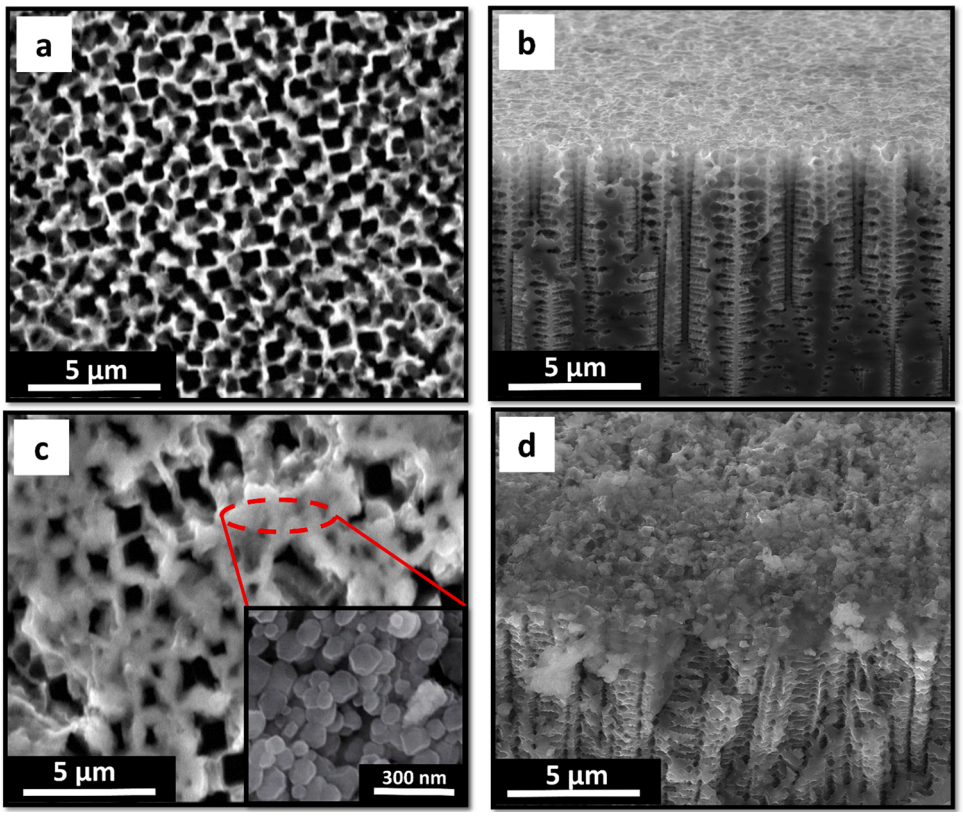

Fig. 2. The planar and cross-sectional morphology of porous silicon substrate and ZIF-67/PS structure.

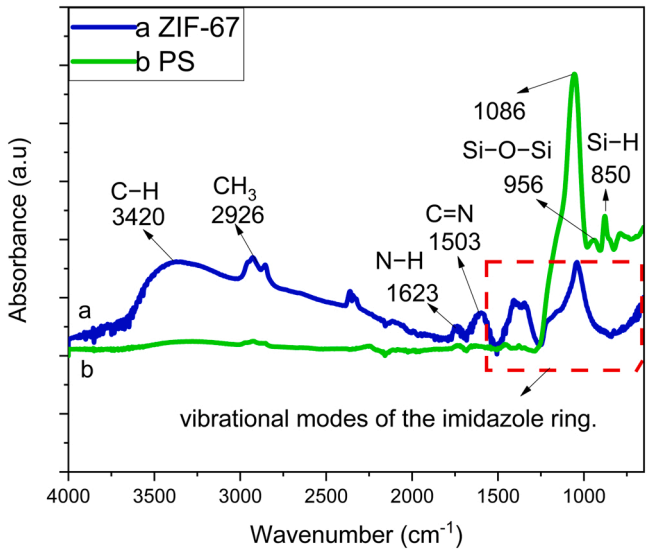

Fig. 3. The attenuated total reflectance (ATR) absorbance spectra of ZIF-67/PS and bare PS samples.

on top of the walls of PS (100) substrate.

Fig. 2 illustrates the FESEM micrographs of the optimized PS and ZIF-67 nanostructures on the PS substrate. For the PS substrate, a nearly uniform distribution of pores with a pore size of ~ 800 nm can be observed. Here, the pores were substantially wide and randomly distributed on the entire porous substrate. The cross-sectional view of the as-prepared PS sample shown in Fig. 2(b) indicates that the Si walls are distinguished from the pin-shaped sharp holes with lengths of up to 20 µm in the Si substrate. Fig. 2(c) shows the planar view of the ZIF/PS sample. As seen, the ZIF-67 structures are homogeneously formed on the porous skeleton of PS. The shape of pores for the ZIF samples followed the morphology of porous substrate with wider pores and thicker walls. The walls in the PS structure provide sufficient nuclei for epitaxial growth of ZIF structures, leading to its rapid crystallization on top of the walls and hence, the formation of porous-shaped ZIF structures. These observations are in good agreement with XRD results which indicated that the structural properties of PS remained intact after deposition of ZIF layers. The cross-sectional view of the ZIF-67/PS sample (Fig. 2d) confirmed that the entire surface of the PS sample is covered by ZIF layers with a thickness of ~ 230 nm. Based on the planar and cross-sectional views, the ZIF structures on the PS substrate are homogeneous, compact, and continuous.

Fig. 3 presents the results of attenuated total reflectance (ATR) spectra of the PS and ZIF-67/PS samples in the wavenumber range of 4000–600 cm^{-1}. For the PS sample, the peak at 850 cm^{-1} can be attributed to Si–H termination, while the peaks at 956 cm^{-1} and 1086 cm^{-1} could be assigned to the Si–O–Si symmetrical bond tension [20]. Concerning the ZIF-67/PS sample, the absorption peaks at 650–1550 cm^{-1} can be ascribed to the vibrational modes of the imidazole rings [21]; while the peaks at 2926 and 1503 cm^{-1} correspond to the tensile modes of the CH_3 and C═N bonds of the ring, respectively [22]. The peak at 1623 cm^{-1} can be attributed to the N–H stretching vibration. The wide peak at 3420 cm^{-1} is attributable to the C–H aromatic stretching mode in ZIF structures [19]. For this sample, the appearance of an absorption peak at 1086 cm^{-1} (related to the Si–O–Si termination) is due to the PS substrate. The ATR results, thus, confirmed the existence of ZIF-67 structures on the PS substrate. Moreover, the optical properties of PS substrate were preserved after ZIF formation which is in good agreement with SEM and XRD findings.

The optical properties of pristine and porous-shaped ZIF structures were assessed through the reflectance spectra of ZIF-67 on different substrates of PS and pristine Si as shown in Fig. 4. To this end, the samples were exposed to UV and visible radiations followed by

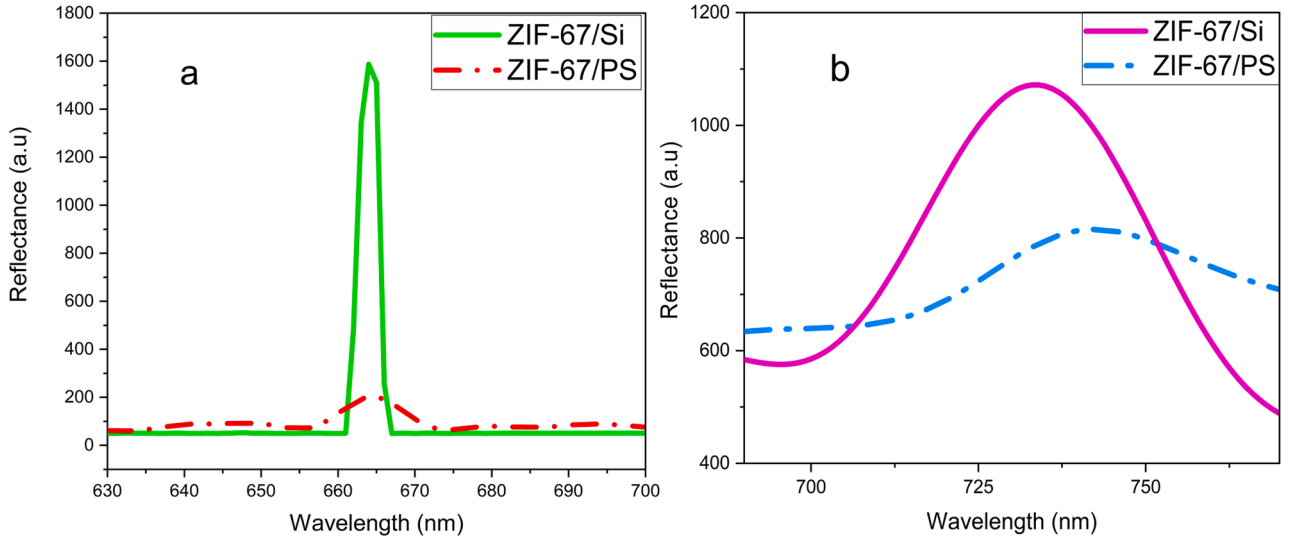

Fig. 4. The reflection spectra of ZIF-67/PS and ZIF-67/Si samples under (a) UV illumination and (b) visible light.

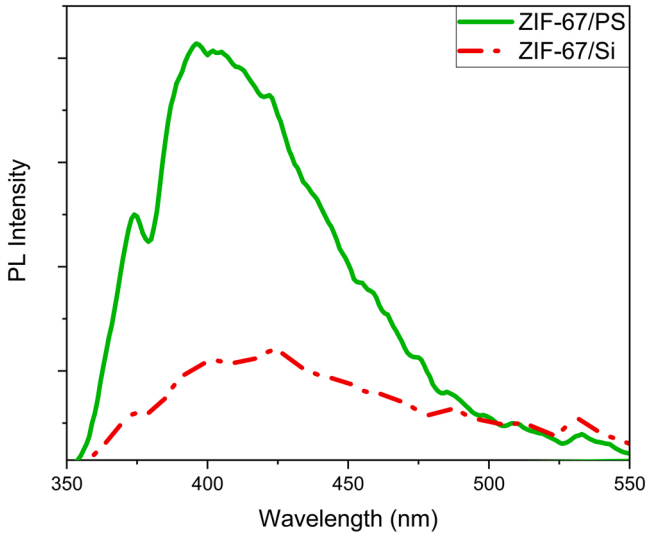

Fig. 5. The photoluminescence spectra of porous-shaped ZIF-67/PS and plain ZIF-67/Si samples.

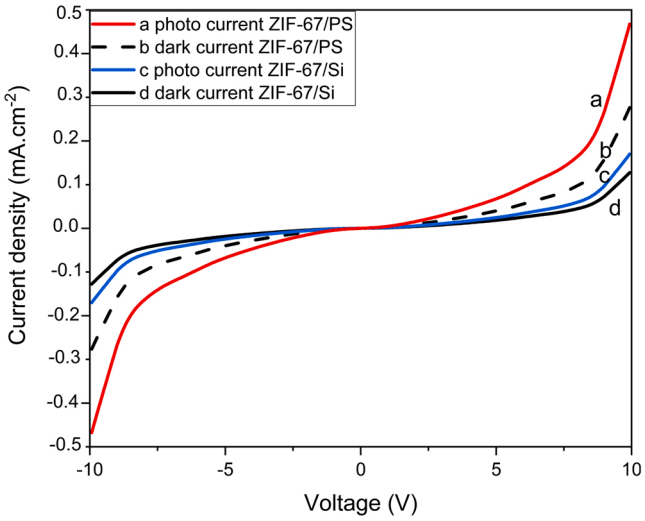

Fig. 6. The current-voltage curves of the MSM photodetectors based on flat ZIF-67/Si and porous-shaped ZIF-67/PS under UV illumination with the wavelength of 365 nm at RT.

recording their reflection spectra. Under UV illumination (Fig. 4a), a noticeable reflectance peak can be observed in the case of the ZIF-67/Si sample. A remarkable reduction (~ 80%) can be, however, detected in porous-shaped ZIF samples on PS nanostructures, suggesting the enhanced UV absorption of porous-shaped ZIF samples compared to the plain ones. The light-capturing in porous shaped ZIF-67/PS sample under visible illumination (Fig. 4b) is obvious in its reflection spectra as compared with the plain ZIF-67/Si sample. A ~ 50% decrease can be observed in the reflection spectra of the porous-shaped sample. Such a lower reflection coefficient of this sample in the UV and visible ranges can be assigned to the higher surface area of the porous-shaped ZIF-67/PS sample which improved its light trapping characteristics. This sample could be thus a proper candidate for optoelectronic devices requiring elevated light absorption.

Fig. 5 shows the room temperature PL emission spectra of porous shaped ZIF-67/PS and plain ZIF-67/Si samples under an excitation wavelength of 300 nm. In MOFs, the emitted wavelength depends on the type and concentration of metal ions, ligand structure, and temperature. The structural properties, environmental effects, porosity, and non-covalent interactions also play a decisive role in the luminescence of MOFs. Linkers in MOFs are generally aromatic units that work with carboxylate groups to coordinate metal and ligands. The emission from aromatic units can be transferred to the visible range due to n-π* and/or π-π* [23]. Also, molecules are enclosed in organic frameworks, allowing charge transfer from organic ligands. In the ligands, the charge transfer energy is inversely related to the oxidation number of the central atom. This implies that the higher the oxidation number of the central metal, the easier the electron transfer from the ligand [24].

For both ZIF-67 samples, the dominant PL peak at 425 nm can be attributed to ligand-ligand charge transfer (LLCT). Because the amount of deposited ZIF layer in the both samples is equal, the increased PL emission in the porous-shaped ZIF-67/PS sample is related to its higher absorption coefficient that is due to its higher surface roughness which led to the greater rate of electron-hole generation. Therefore, the intensity of the PL peak is higher for this sample compared to the plain ZIF-67/Si. The FWHM of the PL peak of the ZIF-67/PS nanostructures and plain ZIF-67/Si was 71 and 82 nm, respectively. The width of the PL maximum is a suitable indicator of material quality in terms of optical properties as the PL peak can easily be broadened by impurities or

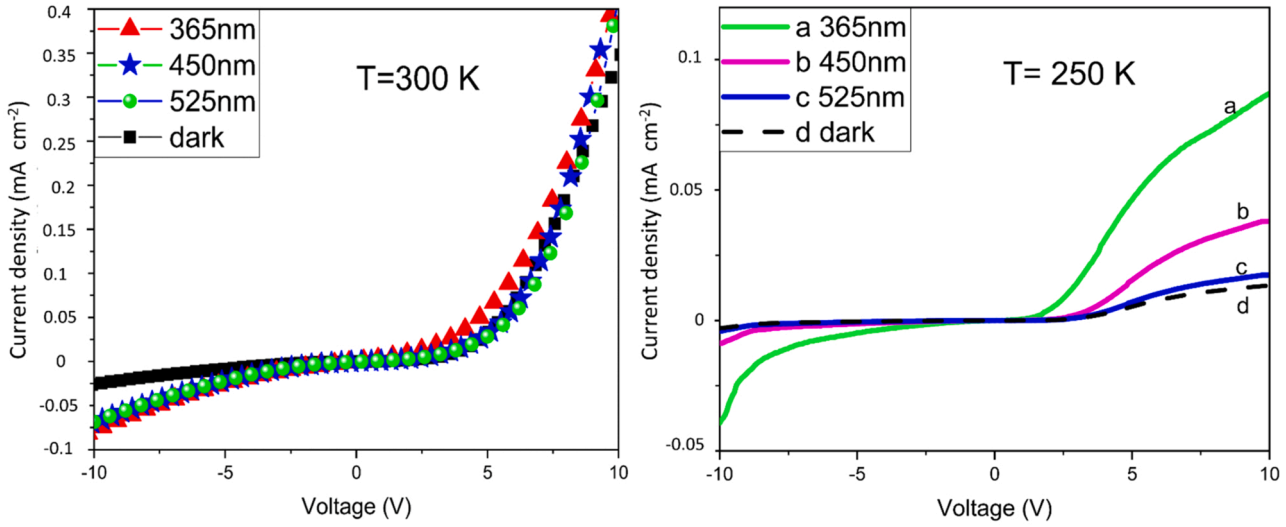

Fig. 7. The I-V curves for the devices based on ZIF-67/PS under different incident wavelengths at 300 and 250 K.

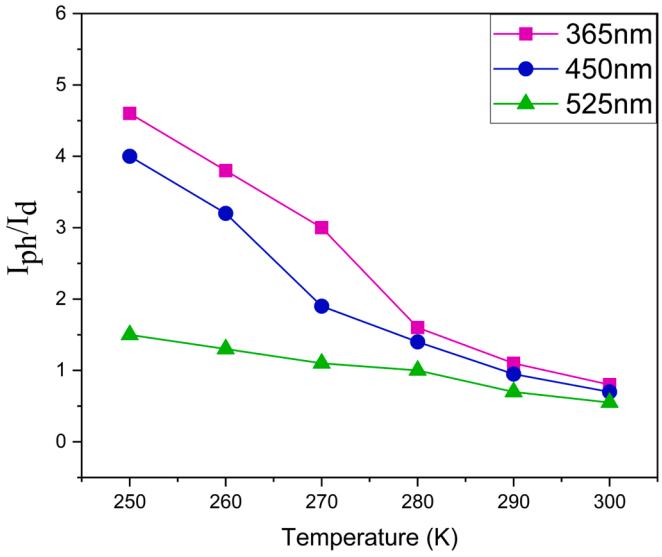

Fig. 8. The electrical gain (I_{Ph}/I_d) of photodetectors fabricated based on ZIF-67/PS nanostructures versus temperature under various wavelengths.

structural defects due to the establishment of different interbands, causing electron transfer with different energies [25]. Accordingly, the concentration of impurities and defects was lower in porous-shaped ZIF structures compared to the flat ZIF sample.

To investigate the optoelectrical properties of ZIF nanostructures, the current–voltage (*I–V*) characteristics of fabricated MSM UV detectors were measured at darkness (I_d) and under UV illumination (I_{Ph}) with the wavelength of 365 nm. Fig. 6 shows the *I–V* curves of the devices based on porous-shaped and flat ZIF samples at RT. Upon exposure to photon, the porous-shaped sample showed a tremendous response to produce significant free carriers for enhanced current conduction. The degree of change in current for this sample was higher than the one based on flat ZIF-67. It indicates the enhanced sensitivity of the fabricated UV detectors based on ZIF-67/PS which is due to the higher photon absorption in this sample. Afterwards, the temperature-dependent electrical characteristics of fabricated devices based on ZIF-67/PS were tested and compared at 250 K and 300 K. Fig. 7 shows a comparison of the two curves at different temperatures which indicates the lower dark current at 250 K (compared to room temperature). The reason for this phenomenon is the intermolecular process of charge transfer in organic semiconductors which takes place from ligand to ligand and in defects and irregularities of the network or potential wells. Thus, the heat-induced vibration of the network will enhance the electron transfer from one molecule to the adjacent ones and consequently increase the dark current. At both temperatures, the photocurrent increased by declining the incident wavelength. However, the difference between photocurrent and dark-current is more significant at lower temperatures (250 K). This observation demonstrates the potential of ZIF/PS structures to detect UV illumination at lower temperatures. Here, the porous skeleton of PS substrate which was followed by the ZIF top layer served as a light-trapping layer and enhanced the rate of electron-hole pair generation, thus improving the performance of the fabricated device.

The effect of temperature on the optoelectrical performance of fabricated photodetectors was further explored by varying the temperature from 250 to 300 K and measuring the current gain (I_{Ph}/I_d) of devices as summarized in Fig. 8 which shows the temperature-dependent behavior of the fabricated photodetector under different wavelengths. At all wavelengths, the current gain significantly increased with decreasing the temperature. At higher temperatures, the difference between I_{Ph} and I_d was negligible. For instance, under UV radiation (λ = 365 nm), the ratio of photocurrent to the dark current was 4.5 and 0.15 at 250 and 300 K, respectively. However, the fabricated device showed minimum response to the higher wavelengths (i.e., 525 nm). The influence of temperature variation was not significant under larger wavelengths of the visible range.

The charge transfer in organic semiconductors occurs through two mechanisms; band-to-band transition under illumination and ligand-to-ligand transition in the darkness. At lower temperatures, the molecular transitions are reduced, hence, the dark current is decreased. Here, the only mechanism for charge transfer was band-to-band transition which was facilitated under illumination at lower wavelengths. At elevated temperatures, the molecular transitions reduced the band-to-band transitions and decreased the electron-hole pair generation. Thus, photocurrent and dark-current were nearly similar at high temperatures. The mobility of band transfer in organic semiconductors is reversely proportional to the absolute temperature which can be obtained through the following equation [26].

$$\mu \propto T^{-n} \; n = 1, 2, 3 \tag{1}$$

In the above equation, n shows the dimension of organic nanostructures. At lower temperatures, the mobility of band transitions is increased, while the molecular transitions show a decline leading to an enhancement in light sensitivity at lower temperatures.

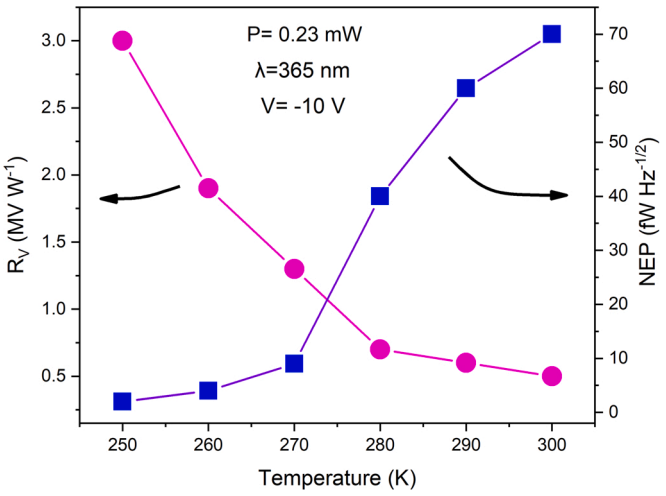

Fig. 9. The temperature-dependence behavior of voltage responsivity (R_V) and the noise equivalent power (NEP) for the fabricated photodetectors based on ZIF-67/PS.

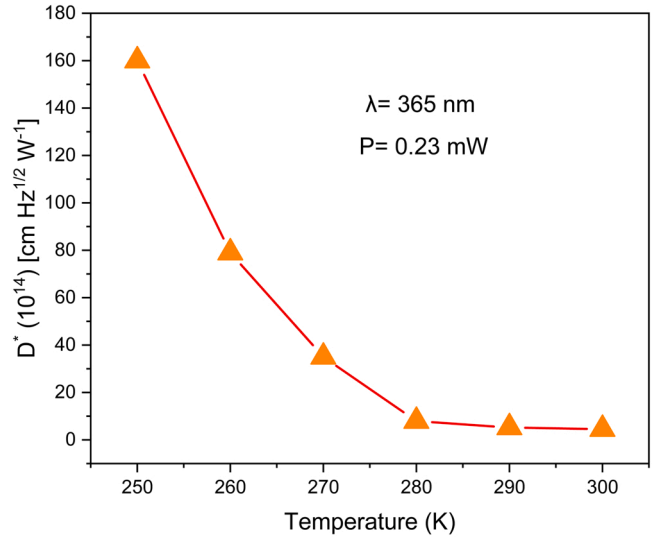

Fig. 10. The temperature dependence of UV detection capability at 10 V bias and wavelength of 365 nm.

One of the most important parameters in the performance of a photodetector is its photoresponse. The responsivity of a photodetector can be determined by [27];

$$R = I_{Ph}/P \times A \tag{2}$$

where P is the power of incident photon, A denotes the exposed area of sensor and R represents the responsivity. For the incident power of 0.23 mW and wavelength of 365 nm, the obtained responsivity is 20 mA W^{-1} at RT.

To assess the influence of temperature on the responsivity, the voltage responsivity (R_V) was defined as the changes in voltage drop per incident power unit across the sensor. At low incident powers, it can be expressed by the following equation;

$$R_V = R \times V/I_d \tag{3}$$

where R shows the value of responsivity and V is the voltage across the device [28]. The R_V value of the fabricated photodetector was 3 and 0.5 MV W^{-1} at 250 and 300 K, respectively. The temperature dependence of voltage responsivity is plotted in Fig. 9. As seen, the voltage drop per unit of incident power was increased in ZIF-67/PS photodetector by reducing the temperature.

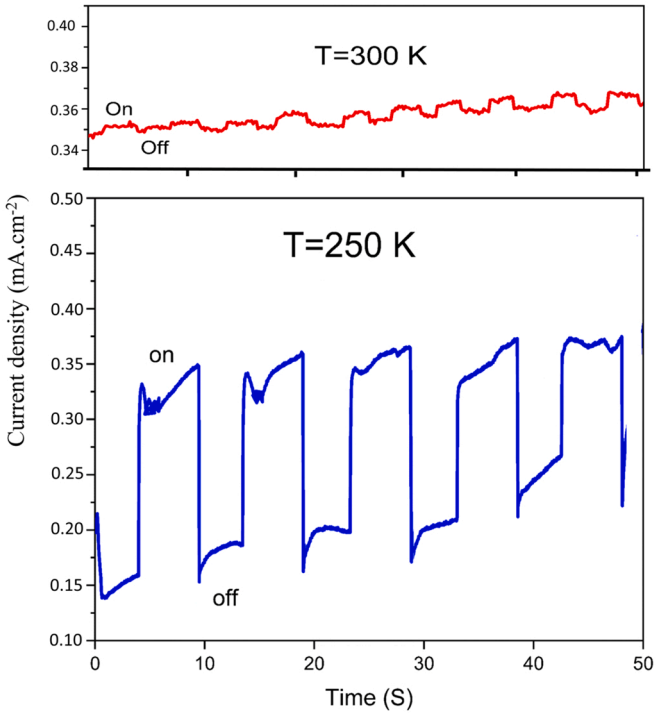

Fig. 11. The consecutive electrical characteristics of fabricated photodetectors under periodic on/off switching of UV illumination at 300 and 250 K.

The noise equivalent power (NEP) can be defined as the lowest optical power required for an output signal-to-noise ratio (I_{Ph}/I_d) for the ZIF-67/PS photodetector according to the following equation:

$$NEP = \sqrt{2eI_d}/R \tag{4}$$

where R is the responsivity, e represents the quantum of charge, and I_d stands for the dark current [29]. The temperature dependence of NEP values is illustrated in Fig. 9. The NEP showed an exponential increment by the temperature elevation. Therefore, the reduced noise values at lower temperatures indicate the better performance of the fabricated devices at lower temperatures.

The detection capability (D*) refers to the ability of the detector to detect the smallest optical signal. D* can be derived from NEP using the following equation:

$$D^* = \sqrt{A}/NEP \tag{5}$$

where A is the exposed area of the photodetector [30]. Fig. 10 shows an increase in the D^* value by temperature decrement. The maximum value of D^* (160×10^{14} cm Hz$^{1/2}$ W^{-1}) was achieved at 250 K.

Fig. 11 depicts the consecutive current curves of the fabricated photodetector in response to the pulsed UV illumination. The fabricated photodetectors were exposed to radiation for a specific duration and allowed to stabilize. The photocurrent was rised to a saturation value under radiation followed by a decline upon switching the UV source off. The rise time was determined as the time taken for the device to achieve 90% of its saturation current; while the recovery time defines as the time taken for the device to reduce its current from maximum to 10% of its saturation current. The rise time at 250 and 300 K were 90 and 250 ms, respectively, while the recovery time was found to be 90 and 160 ms at 250 and 300 K, respectively. Therefore, the detection speed of the ZIF-67/PS-based photodetector was enhanced at lower temperatures, leading to faster photosensitivity.

Table 1
The optoelectrical characteristics of fabricated photodetector based on porous-shaped ZIF-67/PS structures at different temperatures.

Temperature (K)	Current Gain	R_V (MV W^{-1})	NEP (fW $Hz^{-1/2}$)	D* (cm $Hz^{1/2}$ W^{-1})	Rise time (ms)	Recovery time (ms)	BW (Hz)
300	0.8	0.5	70	4.5	250	160	1.4
250	4.6	3	2	160	90	90	3.9

The detector bandwidth (BW) is proportional to the speed of detection and is reversely proportional to the rise time [31];

$$BW(Hz) = 0.349/t_r \quad (6)$$

The bandwidth of the fabricated photodetector was 3.9 and 1.4 Hz at 250 and 300 K, respectively. Table 1 lists the electrical characteristics of the ZIF-67/PS-based photodetector under UV illumination (365 nm) at different temperatures. The elevated band-to-band mobility of charge carriers in organic semiconductors at lower temperatures increased the speed of detection and bandwidth of fabricated photodetectors based on ZIF-67/PS nanostructures. Moreover, deposition of ZIF thin film on porous silicon substrate may improve the stability of PS nanostructures. Theoretically, complete coverage of PS surface by ZIF layers may hinder its exposure to oxygen molecules and prevent the deviation of surface terminations over time. However, this concept should be proved by further experiments.

4. Conclusion

In summary, uniform and high-porosity PS samples were synthesized using electrochemical etching by incorporating Genapol-PF-10 (0.3%v/v) as a surfactant into the electrolyte. The optimized PS sample was chosen as a suitable substrate for the growth of ZIF-67 nanostructures using a solvothermal deposition method. The ZIF-67 structures were homogeneously formed on the porous skeleton of PS. The shape of pores for the ZIF samples appeared to follow the morphology of porous substrate with wider pores and thicker walls. The XRD patterns indicated that the crystalline structure of PS substrate remained intact after deposition of ZIF. The appearance of three peaks at $2\theta = 7.5^\circ$, 10°, and 12.5° indicated the formation of pristine ZIF-67 structures on the top of PS skeleton. The dominant peak at $2\theta = 7.5^\circ$ showed (011) as the favorable orientation for ZIF formation on top of the walls of the PS substrate. The optical properties were explored via PL spectroscopy and reflectometry. The intensity of the PL peak for the porous-shaped ZIF-67 on PS substrate was higher than the plane sample on Si which can be due to its higher surface roughness and greater photon absorption. Moreover, the width of PL peak was lower in ZIF-67/PS nanostructures compared to ZIF-67/Si which was due to its uniformity and improved structural quality. This suggests a decline in the concentration of impurities and defects in porous-shaped ZIF structures. Therefore, this sample could be a promising candidate for photodetection applications. The temperature dependence of the photoresponse properties of fabricated photodetectors was systematically examined to assess the optoelectrical performance of the ZIF-67 structures. A significant improvement was achieved in the performance of the photodetector by cooling the device to lower temperatures due to the charge transfer mechanisms in the organic semiconductors. In the case of the porous-shaped ZIF-67/PS, the noise equivalent power and detectivity values at 250 K were 2 fW $Hz^{1/2}$ and 160 cm $Hz^{1/2}$ W^{-1}, respectively. The rise and recovery time under pulsed UV illumination were measured and compared at 250 and 300 K. The findings revealed the high–speed performance of ZIF-67/PS photodetectors at lower temperatures. The calculated bandwidth for the device at 300 and 250 K was 1.4 and 3.9 Hz, respectively, reflecting an improvement in the performance of the photodetector at lower temperatures. Although the findings of this research indicated a promising future for MOF-based photodetectors, further developments are possible through structural engineering of ZIFs and optimization of device configurations.

CRediT authorship contribution statement

Shadi Ghafari: Methodology, Writing – original draft, Investigation, Visualization, Formal analysis. **Nima Naderi:** Project administration, Supervision, Conceptualization, Validation, Writing – review & editing, Resources, Funding acquisition. **Mohamad Javad Eshraghi:** Supervision, Writing – review & editing, Funding acquisition. **Mahmood Kazemzad:** Supervision, Writing – review & editing, Funding acquisition.

Declaration of Competing Interest

The authors declare that they have no known competing financial interests or personal relationships that could have appeared to influence the work reported in this paper.

Acknowledgements

The present study was supported by Materials and Energy Research Center (MERC) through Grant no. 99392008.

References

[1] M. Sharifi, N. Naderi, P. Fallahazad, M.J. Eshraghi, Role of graphene on the optoelectrical stability of photodetectors based on porous silicon, Sens. Actuators A Phys. 310 (2020), 112065, https://doi.org/10.1016/j.sna.2020.112065.
[2] Y. Tian, N. Vankova, P. Weidler, A. Kuc, T. Heine, C. Wöll, Z. Gu, J. Zhang, Oriented growth of in-oxo chain based metal-porphyrin framework thin film for high-sensitive photodetector, Adv. Sci. 8 (2021), 2100548, https://doi.org/10.1002/advs.202100548.
[3] M. Bednorz, G.J. Matt, E.D. Głowacki, T. Fromherz, C.J. Brabec, M.C. Scharber, H. Sitter, N.S. Sariciftci, Silicon/organic hybrid heterojunction infrared photodetector operating in the telecom regime, Org. Electron. 14 (2013) 1344–1350, https://doi.org/10.1016/j.orgel.2013.02.009.
[4] C. Tudisco, G. Zolubas, B. Seoane, H.R. Zafarani, M. Kazemzad, J. Gascon, P.-L. Hagedoorn, L. Rassaei, Covalent immobilization of glucose oxidase on amino MOFs via post-synthetic modification, RSC Adv. 6 (2016) 108051–108055, https://doi.org/10.1039/C6RA19976C.
[5] M. Kalaj, K.C. Bentz, S. Ayala Jr., J.M. Palomba, K.S. Barcus, Y. Katayama, S. M. Cohen, MOF-polymer hybrid materials: from simple composites to tailored architectures, Chem. Rev. 120 (2020) 8267–8302, https://doi.org/10.1021/acs.chemrev.9b00575.
[6] H. Daglar, H.C. Gulbalkan, G. Avci, G.O. Aksu, O.F. Altundal, C. Altintas, I. Erucar, S. Keskin, Effect of metal–organic framework (MOF) database selection on the assessment of gas storage and separation potentials of MOFs, Angew. Chem. 133 (2021) 7907–7916, https://doi.org/10.1002/ange.202015250.
[7] Y. Zhang, S. Yuan, G. Day, X. Wang, X. Yang, H.-C. Zhou, Luminescent sensors based on metal-organic frameworks, Coord. Chem. Rev. 354 (2018) 28–45, https://doi.org/10.1016/j.ccr.2017.06.007.
[8] F.X.L.i. Xamena, A. Abad, A. Corma, H. Garcia, MOFs as catalysts: activity, reusability and shape-selectivity of a Pd-containing MOF, J. Catal. 250 (2007) 294–298, https://doi.org/10.1016/j.jcat.2007.06.004.
[9] M. Aghayi-Anaraki, V. Safarifard, Fe_3O_4@MOF magnetic nanocomposites: synthesis and applications, Eur. J. Inorg. Chem. 2020 (2020) 1916–1937, https://doi.org/10.1002/ejic.202000012.
[10] J.W.M. Osterrieth, D. Fairen-Jimenez, Metal–organic framework composites for theragnostics and drug delivery applications, Biotechnol. J. 16 (2021), 2000005, https://doi.org/10.1002/biot.202000005.
[11] W.P. Lustig, S. Mukherjee, N.D. Rudd, A.V. Desai, J. Li, S.K. Ghosh, Metal–organic frameworks: functional luminescent and photonic materials for sensing applications, Chem. Soc. Rev. 46 (2017) 3242–3285, https://doi.org/10.1039/C6CS00930A.
[12] Q.-Q. Zhu, Q.-S. Zhou, H.-W. Zhang, W.-W. Zhang, D.-Q. Lu, M.-T. Guo, Y. Yuan, F. Sun, H. He, Design and construction of a metal–organic framework as an efficient luminescent sensor for detecting antibiotics, Inorg. Chem. 59 (2020) 1323–1331. ⟨https://pubs.acs.org/doi/10.1021/acs.inorgchem.9b03032⟩.
[13] J. Troyano, A. Carné-Sánchez, C. Avci, I. Imaz, D. Maspoch, Colloidal metal–organic framework particles: the pioneering case of ZIF-8, Chem. Soc. Rev. 48 (2019) 5534–5546, https://doi.org/10.1039/C9CS00472F.

[14] J. Peng, H. Zhang, Y. Yan, Preparation and characterization of a novel ZIF-8 membrane over high voidage paper-like stainless steel fibers, J. Solid State Chem. 269 (2019) 203–211, https://doi.org/10.1016/j.jssc.2018.09.031.
[15] J. Salonen, E. Mäkilä, Thermally carbonized porous silicon and its recent applications, Adv. Mater. 30 (2018), 1703819, https://doi.org/10.1002/adma.201703819.
[16] N. Naderi, M.R. Hashim, Nanocrystalline SiC sputtered on porous silicon substrate after annealing, Mater. Lett. 97 (2013) 90–92, https://doi.org/10.1016/j.matlet.2013.01.102.
[17] S. Mahmoudi, M.J. Eshraghi, B. Yarmand, N. Naderi, Investigating the effect of phosphorus concentration on the performance of porous silicon solid state solar cells, J. Adv. Mater. Technol. 8 (2019) 65–71, https://doi.org/10.30501/JAMT.2019.88951.
[18] M. Taherkhani, N. Naderi, P. Fallahazad, M.J. Eshraghi, A. Kolahi, Development and optical properties of ZnO nanoflowers on porous silicon for photovoltaic applications, J. Electron. Mater. 48 (2019) 6647–6653, https://doi.org/10.1007/s11664-019-07484-0.
[19] H. Zhou, M. Zheng, H. Tang, B. Xu, Y. Tang, H. Pang, Amorphous intermediate derivative from ZIF-67 and its outstanding electrocatalytic activity, Small 16 (2020), 1904252, https://doi.org/10.1002/smll.201904252.
[20] S. Arshavsky-Graham, K. Urmann, R. Salama, N. Massad-Ivanir, J.-G. Walter, T. Scheper, E. Segal, Aptamers vs. antibodies as capture probes in optical porous silicon biosensors, Analyst 145 (2020) 4991–5003, https://doi.org/10.1039/D0AN00178C.
[21] W.M.A. El Rouby, M. Antuch, S.-M. You, P. Millet, Surface sensitization of TiO_2 nanorod mats by electrodeposition of ZIF-67 for water photo-oxidation, Electrochim. Acta 339 (2020), 135882.
[22] V.K. Abdelkader-Fernández, D.M. Fernandes, S.S. Balula, L. Cunha-Silva, C. Freire, Advanced framework-modified POM@ZIF-67 nanocomposites as enhanced oxygen evolution reaction electrocatalysts, J. Mater. Chem. A 8 (2020) 13509–13521.
[23] M. Moradi, N. Naderi, First principle study of hydrogen storage on the graphene-like aluminum nitride nanosheet, Struct. Chem. 25 (2014) 1289–1296, https://doi.org/10.1007/s11224-014-0410-x.
[24] X. Li, S.S. Rajasree, J. Yu, P. Deria, The role of photoinduced charge transfer for photocatalysis, photoelectrocatalysis and luminescence sensing in metal–organic frameworks, Dalton Trans. 49 (2020) 12892–12917, https://doi.org/10.1039/D0DT02143A.
[25] V. Adinolfi, W. Peng, G. Walters, O.M. Bakr, E.H. Sargent, The electrical and optical properties of organometal halide perovskites relevant to optoelectronic performance, Adv. Mater. 30 (2018), 1700764.
[26] J. Singh, M.R. Narayan, D. Ompong, Theory of optical properties of organic semiconductors, Org. Semicond. Optoelectron. (2021) 69–92, https://doi.org/10.1002/9781119146131.ch3.
[27] M. Moghaddam, N. Naderi, M. Hosseinifard, A. Kazemzadeh, Improved optical and structural properties of cadmium sulfide nanostructures for optoelectronic applications, Ceram. Int. 46 (2020) 7388–7395, https://doi.org/10.1016/j.ceramint.2019.11.234.
[28] H. Arora, R. Dong, T. Venanzi, J. Zscharschuch, H. Schneider, M. Helm, X. Feng, E. Cánovas, A. Erbe, Demonstration of a broadband photodetector based on a two-dimensional metal–organic framework, Adv. Mater. 32 (2020), 1907063, https://doi.org/10.1002/adma.201907063.
[29] M.Z. Nawaz, L. Xu, X. Zhou, K.H. Shah, J. Wang, B. Wu, C. Wang, CdS nanobelt-based self-powered flexible photodetectors with high photosensitivity, Mater. Adv. 2 (2021) 6031–6038, https://doi.org/10.1039/D1MA00580D.
[30] Y. Ma, D. Liu, J. Hao, L. Wang, W. Wang, High-performance flexible WSe_2 flake photodetector with broadband detection capability, AIP Adv. 10 (2020), 125027, https://doi.org/10.1063/5.0033483.
[31] G.C. Amaral, L.E.Y. Herrera, P. Tovar, E.F. Carneiro, J.P. von der Weid, P.J. Urban, Single-tone multiple copper line monitoring in frequency-reusable fiber-extended copper line architectures, in: Proceedings of the 2017 Int., ⟨https://doi.org/10.1109/MWP.2017.8168664⟩.

Shadi Ghafari: She is an MSc student in thin film physics at Materials and Energy Research Center (MERC). Her research interests include design, fabrication and characterization of nanomaterials, porous materials, photodetectors, and MOFs-based devices.

Nima Naderi: He is a semiconductor science researcher, materials specialist and solid state physicist. He received his PhD from Universiti Sains Malaysia (USM), Malaysia. His research interests include photonic materials, two-dimensional semiconductors and optoelectronic devices. He is currently a faculty member at Materials and Energy Research Center (MERC).

Mohamad Javad Eshraghi: He is a solid state physicist. His research interests include coating processes and surface engineering of materials for improving electrical properties and magnetic behavior of thin films. He is currently a faculty member at Materials and Energy Research Center (MERC).

Mahmood Kazemzad: He is an Associate Professor of Materials Chemistry at Materials and Energy Research Center. He got MSc in Physical Chemistry (Electrochemistry) and Ph. D. in Material Science. His multidisciplinary research is related to syntheses and applications of nanostructured materials in sensors, catalysts and adsorbents. He is expert in laboratory scale preparation and characterization of Zeolites, MOFs and mesoporous metal oxides.